TRANSIENT HEAT TRANSFER OF HYDROMAGNETIC VARIABLE ELECTRIC CONDUCTIVITY JOULE HEATING FLUID PAST A DARCY-FORCHHEIMER POROUS INCLINED CYLINDER MEDIUM

Supported by tetfund TERTIARY EDUCATION TRUST FUND

O. K. Onanuga[1]*, M. A. C. Chendo[2] and N. E. Erusiafe[2]
[1]Department of Physics, Lagos State Polytechnic, Ikorodu, Nigeria
[2]Department of Physics, University of Lagos, Akoka, Lagos State, Nigeria
*Corresponding author: eogoko@noun.edu.ng

Received: December 03, 2017 **Accepted:** March 09, 2018

Abstract: In this study, analysis of transient free convective Joule heating flow of viscous dissipation and radiative heat transfer in an inclined Darcy-forchhemier porous cylinder medium with the constant uniform source or sink and variable electric conductivity is considered. The Rosseland approximation is adopted for the expression of thick radiation heat flux in the heat equation with gray radiating liquid, non-scattering but with absorbing-emitting depending on wavelength. The boundary layer coupled nonlinear governing system of partial differential equations are non-dimensional and solved using unconditionally stable, compatible and convergence implicit finite difference scheme of Crank-Nicolson type. The computational results are obtained and presented graphically to illustrate all the embedded parameters in the transient momentum and energy equations. The flowing liquid and heat transfer characteristics at the plate which are of engineering interest are examined and discussed for the skin-friction coefficient and thermal gradient as shown graphically.

Keywords: Darcy-forchheimer, heat transfer, hydromagnetic, Joule heating, variable electric conductivity

Introduction

The analysis of fluid flow in a cylinder which involves the interaction of numerous occurrences has a wide area of applications in the field of space sciences, engineering and technology. One such study is associated with the significance of free convection magnetohydrodynamic (MHD) flow which shows an essential character in petroleum industries, engineering, and agriculture. The study under investigation has vital applications in examining the geological formations; in the thermal oil recovery and exploration; and in the assessment of underground waste nuclear storage, geothermal reservoirs and aquifers. Hossain (1988) reported on a semi-infinite vertical plate of two-dimensional heat and mass transfer free convection flow. An integral scheme was adopted to obtain a solution for lower velocity and temperature amplitude at the wall.

Many scholars have examined the natural boundary layer convective flow of an electrically conducting liquid in the occurrence of a magnetic field. Emerly-Ashly (1963) studied the consequence of magnetic field on free convection boundary layer flows. An exact solution for the magnetohydrodynamic flow was obtained for rotating cylinders in a radial magnetic field by Arora and Gupta (1972). The energy and species transfer influences on the flow through an oscillating surface with variable temperature was examined by Soundalgekar *et al*. (1994). It was noticed from the results that the skin friction rose with a rise in the ωt. Kumari and Nath (1999) investigated the formation of asymmetric viscous fluid hydrodynamic in a stagnation point flow of a 2D body over an extending plate when the fluid was in a continuous motion from rest. Due to its several applications, consequence of radiation on the flow of hydrodynamic induced by an inclined stretching cylinder with non-uniform heat source/sink was carried out by Hayat *et al*. (2017) while analytical study was carried out involving permeable plates with an inclined magnetic poiseuille fluid flow by Manyonge *et al*. (2012). Inclined magnetic field with chemical reaction effects on the semi-infinite porous surface through a permeable media was examined by Sugunamma *et al*. (2013). It was noticed that the velocity decreased as the inclined magnetic field and Hartmann number increases. Radiation heat transfer is critical in the formation of reliable tools, gas turbines and many impulsion devices for space vehicles, satellites, nuclear plants and aircraft missiles.

Similarly, the effects of thermal radiation and viscous dissipation on the free convection flows are substantial in astronomical technology and processes involving high heat Dulal and Hiranmoy (2012). Analysis of velocity slip and thermal radiation temperature jump towards stretched plate under the influence of heat transport was considered by Zheng *et al*. (2013), while Sheikholeslami *et al*. (2015) studied the radiation phenomena and magnetohydrodynamic flow of nano-fluid. Hayat *et al*. (2015) examined heat absorption or generation and thermal radiation impacts on stagnation point flow of tangent hyperbolic fluid in the existence of convective heat and species transfer. Hayat *et al*. (2016a, 2016b) reported on the properties of heat source/sink and radiation in the magnetohydrodynamic flow of nano-fluid. Some fascinating studies for time series analysis and two-phase flows were reported on by Gao *et al*. (2015a, 2015b, 2016a, 2016b and 2016c).

An analytical and experimental study is presented by Evans *et al*. (1968) for unsteady free convection in a vertical cylinder. The cylinder experimental was subjected to an unvarying temperature flux at the walls while an analytical formulation was modeled. The heat of the primary fluid was taken to differ in the perpendicular direction nevertheless not in the horizontal path. Finite difference solution of transient radiative magnetohydrodynamic flow of heat and mass transfer past a cylinder was analyzed by Ismail *et al*. (2012). Lately, Velusamy and Garg (1992) gave a computational solution for the transient thermal capacities and radii in a cylinder with the heat source. A completely implicit finite difference method was adopted solving the nonlinear coupled equations. The frequency of spread of the principal edge effect was given special attention. They established that the rate forecast by the one-dimensional conveyance solution was slower than that obtained from the boundary layer solution. The transient boundary layer thickness was gotten to surpass its steady-state values. Unsteady MHD convection flow of heat and mass transfer through a vertical cylinder was investigated by Periyana and Ponnamma (2000). Finite difference solution of unsteady chemical reaction MHD convective heat oscillation flow past motioning semi-infinite cylinder was examined by Rajesh *et al*. (2016).

However, to the best knowledge of the research, little or no research work has been done on transient dissipative variable electric conductivity and thermal radiation in a Joule heating with free convective flow past an inclined non-Darcy porous cylinder medium under the influence of heat transfer. As a result, the objective of the current study is to examine the unsteady free convective hydrodynamic viscous dissipation and incompressible fluid flow through a porous medium of a cylinder under the stimulus magnetic field and radiation. Thus, an important change in the momentum and temperature was noticed. The mathematical formulation of the model is shown in section two. In section three, the implicit finite difference method of Crank-Nicolson type and its application is presented in space for the computation. In section 4, the numerical with the graphical results are illustrated and quantitatively discussed with respect to embodiment fluid parameters present in the flow.

Mathematical Formulation

Consider unsteady laminar, incompressible radiative and viscous dissipative heat transfer of variable electric conductivity fluid flow in a non-Darcy porous cylinder medium with joule heating and uniform heat absorption/generation. The hydrodynamic incompressible fluid flow through an inclined semi-infinite cylinder in the range $0 < x < \frac{\pi}{2}$. Here the x-axis is assumed along the cylinder axis in the inclined direction and the radius of the coordinate r is perpendicular to the cylinder. All physical characteristics are taken to be unchanged except for the density in the buoyancy term, as considered in the usual Boussinesq approximation. Under these assumptions, the flow geometry model and coordinate system together with the equations governing the conservative law, momentum and energy are as follow:

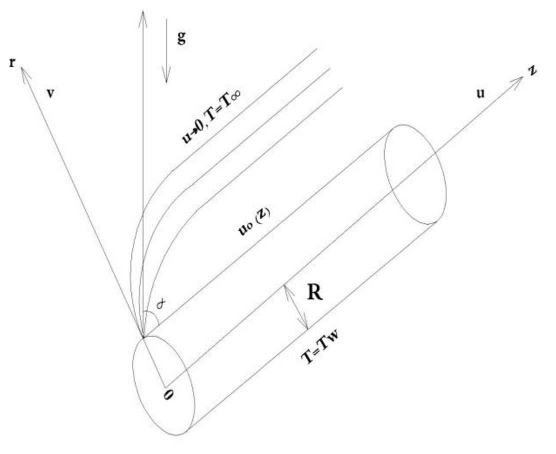

Fig. 1: Physical model and coordinate system

$$\frac{\partial(ru)}{\partial x} + \frac{\partial(rv)}{\partial r} = 0 \qquad (1)$$

$$\frac{\partial u}{\partial \bar{t}} + u\frac{\partial u}{\partial x} + v\frac{\partial u}{\partial r} = \frac{\nu}{r}\frac{\partial}{\partial r}\left(r\frac{\partial u}{\partial r}\right) - \frac{\sigma(B(x))^2 u}{\rho} + g\beta(T-T_\infty)cos\alpha - \frac{\nu}{k_0}u - \frac{b}{k_0}u^2 \qquad (2)$$

$$\frac{\partial T}{\partial \bar{t}} + u\frac{\partial T}{\partial x} + v\frac{\partial T}{\partial r} = \frac{k}{\rho c_p}\frac{1}{r}\frac{\partial}{\partial r}\left(r\frac{\partial T}{\partial r}\right) - \frac{1}{\rho c_p}\frac{1}{r}\frac{\partial}{\partial r}(rq_r) + \frac{\nu}{c_p}\left(\frac{\partial u}{\partial r}\right)^2 + \frac{\sigma(B(x))^2}{\rho c_p}u^2 + \frac{Q(T-T_\infty)}{\rho c_p} \qquad (3)$$

Subject to no-slip boundary conditions

$$\begin{aligned} &\bar{t} \le 0: u = 0, v = 0, T = T_\infty,\ for\ \ x \ge 0\ \ and\ \ r \ge 0 \\ &\bar{t} > 0: u = u_0, v = 0, T = T_w,\ at\ \ r = r_0 \\ &u = 0, T = T_\infty,\ at\ \ x = 0 \\ &u \to \infty, T \to \infty, r \to \infty \end{aligned} \qquad (4)$$

In this investigation, it is taken that the used magnetic field strength $B(x)$ varies and it is illustrated as $B(x) = \frac{B_0}{\sqrt{x}}$, where B_0 is unchanged. Also, the electrical conductivity σ relies on the velocity of the fluid and it can be defined as $\sigma = \sigma_0 u$, for σ_0 is constant, see Salawu and Fatunmbi (2017). that is,

$$B(x) = \frac{B_0}{\sqrt{x}}\ \ and\ \ \sigma = \sigma_0 u \qquad (5)$$

The term q_r in equation (3) represents radiation. According to Rosseland diffusion approximation for radiation, q_r can be defined as (Salawu and Amoo (2016));

$$q_r = -\frac{4\sigma'}{3\delta}\frac{\partial T^4}{\partial r} \qquad (6)$$

Where: σ' and δ are the Stefan-Boltzmann and the mean absorption coefficient respectively. Assuming heat difference in the flow is satisfactory low such that T^4 may be written linearly as a function of temperature, applying Taylor series to expand T^4 is expanded about T_∞

$$T^4 \cong T_\infty^4 + 4T_\infty^3(T-T_\infty) + 6T_\infty^2(T-T_\infty)^2 + ... \qquad (7)$$

Neglecting higher-order terms of $T - T_\infty$ in equation (8) to get

$$T^4 \approx 4T_\infty^3 T - 3T_\infty^4 \qquad (8)$$

Using equation (9) on equation (7) to obtain

$$q_r = -\frac{16T_\infty^3\sigma'}{3\delta}\frac{\partial T}{\partial r} \qquad (9)$$

Substituting equations (5) and (9) along with the following non-dimensionless parameters (10) into equations (1) to (4)

$$U = \frac{u}{u_0}, V = \frac{vr_0}{\nu}, X = \frac{x\nu}{u_0 r_0^2}, t = \frac{\bar{t}\nu}{r_0^2}, R = \frac{r}{r_0}, \theta = \frac{T-T_\infty}{T_w - T_\infty} \qquad (10)$$

Therefore, the main governing equations of the flow along with the boundary conditions are now reduced to

$$\frac{\partial U}{\partial X}+\frac{V}{R}+\frac{\partial V}{\partial R}=0 \quad (11)$$

$$\frac{\partial U}{\partial t}+U\frac{\partial U}{\partial X}+V\frac{\partial U}{\partial R}=\frac{1}{R}\frac{\partial U}{\partial R}+\frac{\partial^2 U}{\partial R^2}-MU^2+Gr\theta cos\alpha-FsU-DaU^2 \quad (12)$$

$$\frac{\partial \theta}{\partial t}+U\frac{\partial \theta}{\partial X}+V\frac{\partial \theta}{\partial R}=\frac{1}{Pr}\left(1+\frac{4}{3}N\right)\left(\frac{\partial^2 \theta}{\partial R^2}+\frac{1}{R}\frac{\partial \theta}{\partial R}\right)+Ec\left(\frac{\partial U}{\partial R}\right)^2+EcMU^3+\lambda\theta \quad (13)$$

The corresponding boundary conditions are as follow;

$$\begin{aligned} &t\le 0: U=0, V=0, \theta=0 \;\; for\ all\;\; X\ge 0\ and\ R\ge 0\\ &t>0: U=1, V=0, \theta=1\;\; at\;\; X=0 \qquad (14)\\ &U=0, V=0, \theta=0,\;\; at\;\; X=0\\ &U\to 0, V\to 0, \theta\to 0\;\; as\;\; R\to\infty \end{aligned}$$

Where: $M=\frac{\sigma_0 B_0^2}{X\rho}$ is the magnetic field parameter, $Gr=\frac{gr_0^2\beta(T-T_\infty)}{\nu u_0}$ is the thermal Grashof number, $Fs=\frac{r_0^2}{k_0}$ is the Forchhemier parameter, $Da=\frac{bu_0r_0^2}{k_0\nu}$ is the Darcy number, $Ec=\frac{u_0^2}{c_p(T_w-T_\infty)}$ is the Eckert number, $Pr=\frac{\mu c_p}{k}$ is the Prandtl number, $N=\frac{4T_\infty^3\sigma'}{\delta k}$ is the radiation parameter, $\lambda=\frac{Qr_0^2}{\mu c_p}$ is the heat generation parameter.

The local skin-friction and Nusselt number in the dimensionless quantities form are as follows:

$$\tau_x=-\left(\frac{\partial U}{\partial R}\right)_{R=1} \quad (15)$$

$$\tau=-\int_0^1\left(\frac{\partial U}{\partial R}\right)_{R=1}dX \quad (16)$$

$$Nu_x=-X\left(\frac{\partial \theta}{\partial R}\right)_{R=1} \quad (17)$$

$$Nu=-\int_0^1\left(\frac{\partial \theta}{\partial R}\right)_{R=1}dX \quad (18)$$

The formulations involved in the equations (15) to (18) are established by using Newton-Cotes five-point formula approximation and integrals.

Method of Solution

To obtain the computational results for the unsteady nonlinear coupled partial differential equations (11) to (14), an implicit finite difference Crank-Nicholson algorithm is employed see Ismail (2012). The finite difference algorithms corresponding to equation (11) to (14) are as follows:

For the law of conservation of mass (i.e Continuity equation);

$$\frac{U_{i,j}^{w+1}-U_{i-1,j}^{w+1}+U_{i,j}^{w}-U_{i-1,j}^{w}}{\Delta X}+\frac{V_{i,j}^{w+1}+V_{i,j}^{w}}{1+(j-1)\Delta R}+\frac{V_{i,j+1}^{w+1}-V_{i,j-1}^{w+1}+V_{i,j+1}^{w}-V_{i,j-1}^{w}}{2\Delta R}=0 \quad (19)$$

For the fluid flow momentum equation;

$$\begin{aligned}&\frac{U_{i,j}^{w+1}-U_{i,j}^{w}}{\Delta t}+U_{i,j}^{w}\left(\frac{U_{i,j}^{w+1}-U_{i-1,j}^{w+1}+U_{i,j}^{w}-U_{i-1,j}^{w}}{2\Delta X}\right)+\\ &V_{i,j}^{w}\left(\frac{U_{i,j+1}^{w+1}-U_{i,j-1}^{w+1}+U_{i,j+1}^{w}-U_{i,j-1}^{w}}{4\Delta R}\right)=Gr\left(\frac{\theta_{i,j}^{w+i}+\theta_{i,j}^{w}}{2}\right)cos\alpha+\\ &\frac{U_{i,j-1}^{w+1}-2U_{i,j}^{w+1}+U_{i,j+1}^{w+1}+U_{i,j-1}^{w}-2Ui,j^{w}+U_{i,j+1}^{w}}{2(\Delta R)^2}-M\left(\frac{U_{i,j}^{w+1}+U_{i,j}^{w}}{2}\right)^2\\ &\frac{U_{i,j+1}^{w+1}-U_{i,j-1}^{w+1}+U_{i,j+1}^{w}-U_{i,j-1}^{w}}{4[1+(j-1)\Delta R]\Delta R}-Fs\left(\frac{U_{i,j}^{w+i}+U_{i,j}^{w}}{2}\right)-Da\left(\frac{U_{i,j}^{w+1}+U_{i,j}^{w}}{2}\right)^2\end{aligned} \quad (20)$$

Also, for the temperature equation;

$$\frac{\theta_{i,j}^{w+1}-\theta_{i,j}^{w}}{\Delta t}+U_{i,j}^{w}\left(\frac{\theta_{i,j}^{w+1}-\theta_{i-1,j}^{w+1}+\theta_{i,j}^{w}-\theta_{i-1,j}^{w}}{2\Delta X}\right)+ V_{i,j}^{w}\left(\frac{\theta_{i,j+1}^{w+1}-\theta_{i,j-1}^{w+1}+\theta_{i,j+1}^{w}-\theta_{i,j-1}^{w}}{4\Delta R}\right)=\lambda\left(\frac{\theta_{i,j}^{w+i}+\theta_{i,j}^{w}}{2}\right)+ \left(1+\frac{4}{3}N\right)\left(\frac{\theta_{i,j-1}^{w+1}-2\theta_{i,j}^{w+1}+\theta_{i,j+1}^{w+1}+\theta_{i,j-1}^{w}-2\theta i,j^{w}+\theta_{i,j+1}^{w}}{2Pr(\Delta R)^2}\right)+ \left(1+\frac{4}{3}N\right)\left(\frac{\theta_{i,j+1}^{w+1}-\theta_{i,j-1}^{w+1}+\theta_{i,j+1}^{w}-\theta_{i,j-1}^{w}}{4Pr[1+(j-1)\Delta R]\Delta R}\right)+EcM\left(\frac{U_{i,j}^{w+1}+U_{i,j}^{w}}{2}\right)^3+ Ec\left(\frac{U_{i,j+1}^{w+1}-U_{i,j-1}^{w+1}+U_{i,j+1}^{w}-U_{i,j-1}^{w}}{4\Delta R}\right)^2 \tag{21}$$

Numerical Approach

To obtain the finite difference in the grid and mesh for the equations, the area of integration is assumed as a rectangle contained lines showing $Xmin=0$, $Xmax=1$, $Rmin=1$ and $Rmax=16$, where $Rmax$ relates to $R=\infty$ which is far away from the momentum and thermal boundary layers. In the equations, the subscripts i and j denote the grid points along the X and R coordinates, where $R=1+(j-1)\Delta R$ and $X=i\Delta X$ as well as the superscript w represents the value of time $t\ (=w\Delta t)$, with ΔR, Δt and ΔX denotes the mesh size in the R, t and X axes, respectively. To get a reliable grid system for the analysis, a grid independent test was carried out. The steady-state grid system obtained for the momentum and energy values at 100×500, 50×250 and 200×1000 differ from one and the others in second decimal and fifth decimal place. Therefore, the grid system performed better and it is chosen for all subsequent studies, with a mesh size in R and X direction. More also, the time step size reliance was examined, for which 0.01 gives a consistent result. Considering the initial and boundary conditions are given in the study, the values of velocity U and temperature θ given at the time $t=0$, hence the values of θ, V and U at the next time step can be computed. Largely, when the variables are given at $t=w\Delta t$, the values at $t=(k+1)\Delta t$ can be computed as follows. The finite difference for the velocity and temperature equations at the nodal point on a precise i-level result into a tri-diagonal system of equations. The system of equations is solved by using Thomas algorithm (1969). Firstly, the velocity U and temperature θ are calculated at each j nodal points on i-level at the $(w+1)th$ time step. Then the velocity V is computed from the continuity equation explicitly. This procedure is repeated for the consecutive i-levels; hence the values of U, V and θ at each grid points within the rectangular region are obtained at $(w+1)th$ time step. The iterative algorithm process is repeated for several time steps until a steady-state result is achieved. That is when the difference in the absolute values of the temperature and velocity at all grid points in two successive time steps is less than 10^5. The adopted truncation error for finite difference approximation is $O(\Delta t^2+\Delta R^2+\Delta X^2)\to 0$ as $\Delta X\to 0$, $\Delta R\to 0$ and $\Delta t\to 0$. Therefore, the system is unconditionally stable. Hence, finite difference scheme is compatible and stable. Thus, convergence is ensured.

Results and Discussion

To obtain a clear understanding of the physical problem, it is essential to carry out the computation analysis of the problem for the dimensionless momentum field, energy field, the coefficient of skin friction, and the thermal gradient number by allocating some arbitrarily selected values based on existing literature to the bodily parameters entrenched in the fluid flow. The following diverse computations values as set as the default values for the embedded parameters; $Gr=3, P=0.72, Fs=0.2, \lambda=2, \alpha=0.5, Da=0.5, Ec=0.5, M=0.5, N=0.5\ and\ t=1$. All graphs satisfy the values except otherwise stated on the respective graph.

Figure 2 represents the velocity profile for varying in the values of the magnetic field parameter M. It is noticed that the velocity profiles decreases with an increase in the value of the magnetic field parameter M. This is because the imposition of the transverse magnetic field on an electrically conducting fluid induces a drag-like force known as a Lorentz force on the flow field which acted against the fluid motion and slows it down. Thus, the Lorentz force increases as M increases which then dampens the velocity profiles.

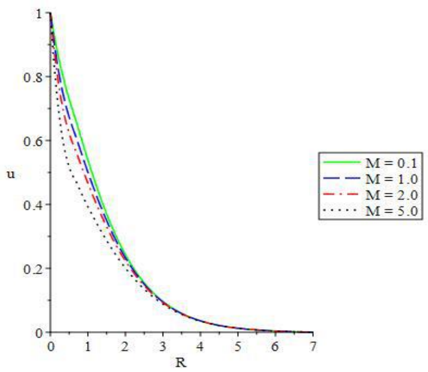

Fig. 2: Transient Velocity for values of M

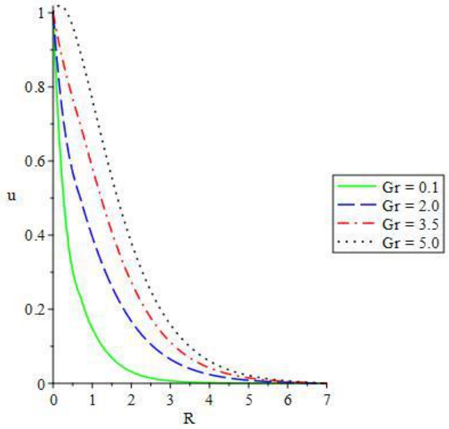

Fig. 3: Transient Velocity for values of Gr

Figure 3 shows the plot of velocity fields against R for various values of thermal Grashof number Gr. It is evidence from these figure that the velocity increases as the magnitude of Gr increases. From the physical point of view, thermal Grashof number is the relative effect of the thermal buoyancy force to the viscous hydrodynamic force in the boundary layer. Thus, the motion of the fluid accelerated by a corresponding increase in Gr. As displayed in this figure, Gr has a greater impact on the velocity near the cylinder surface within the boundary layer.

The impact of the angle of inclination α of the cylinder on the velocity distribution is shown in the Fig. 4. From this figure, it is observed that the fluid velocity increases with an increase in the angle of inclination α, the velocity increases because the gravity is enhanced which resulted in magnifying the buoyancy force and thereby increases the flow momentum in the system. Fig. 5 describes the influence of time and space dependent heat source λ on the heat distribution in the boundary layer. It is noticed that the heat content in the cylinder increases as the space-dependent heat generation when $(\lambda > 0)$ increases. A rise in the velocity field leads to rising in the interaction of the fluid particles that causes rises in the heat energy within the system, this increase in temperature also causes an increase in the flow distribution.

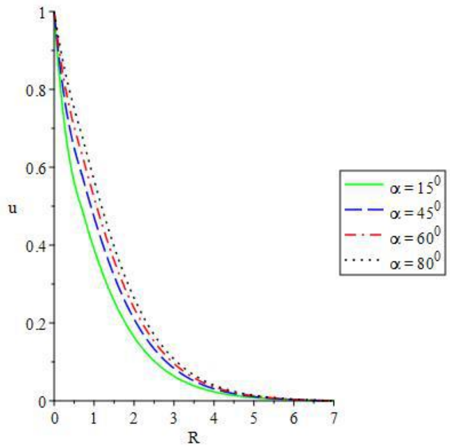

Fig. 4: Transient Velocity for values of α

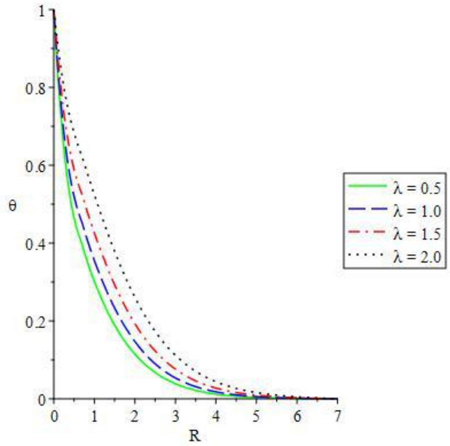

Fig. 5: Transient Temperature for values of λ

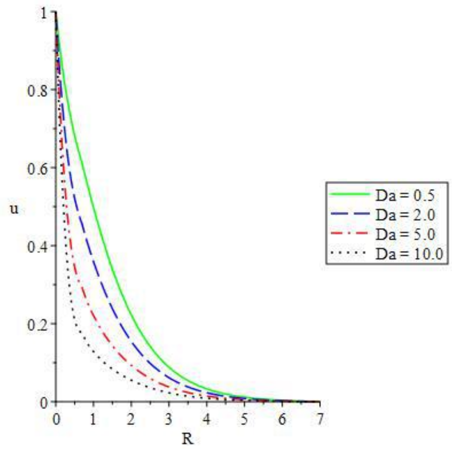

Fig. 6: Transient Velocity for values of Da

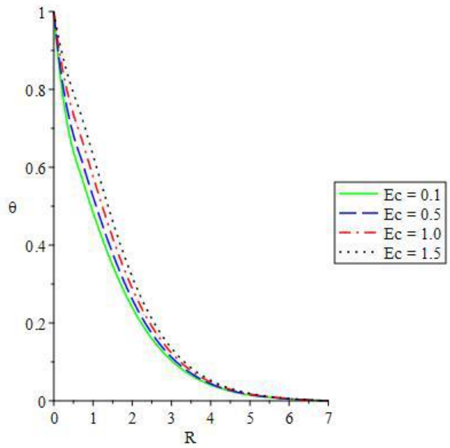

Fig. 7: Transient Temperature for values of Ec

The impact of Darcy parameter Da on the velocity profiles in the cylinder with radius R is displayed in Fig. 6. It is observed that the velocity decreases as the porosity parameter values Da increases. This increase in Darcy parameter Da increases the resistance to the free flow of fluid in the system and thereby retarded the flow motion. As a result of this, the flow fluid velocity diminishes as $R \to \infty$ with the system as seen in the figure. Fig. 7 represents the variation temperature with R for different values of Eckert number Ec. Eckert number is referred to as fluid motioning controlling parameter. It describes the ratio of the kinetic energy of the flow to the boundary layer enthalpy difference, that is, the conversion of kinetic energy into thermal energy by the work done against the viscous fluid stresses. An increase in Ec causes the energy transfer in the cylinder to rises, due to drag between the fluid particles that result in an increase heat production. Thus, additional heat is transferred within the system and the thermal buoyancy force then increase, causing the temperature to rise as displayed in the figure.

Figure 8 illustrates the influence of Prandtl number Pr on the heat distribution when $0.40 \leq Pr \leq 2$. Here, observation reveals that temperature field reduces as Pr increases in the system. The is due to the fact that as Pr increases the fluid temperature and its boundary layer thickness diminish which strengthen fluid bonding forces. In consequence, there is a net reduction in the thermal buoyancy effect of the heat transfer within the cylinder. In addition, increase in Pr is an indication that causes the fluid viscosity to rise.

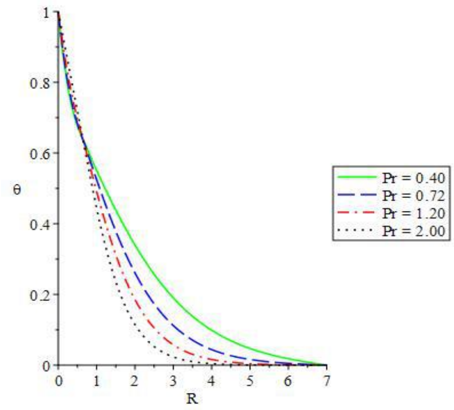

Fig. 8: Transient Temperature for values of Pr

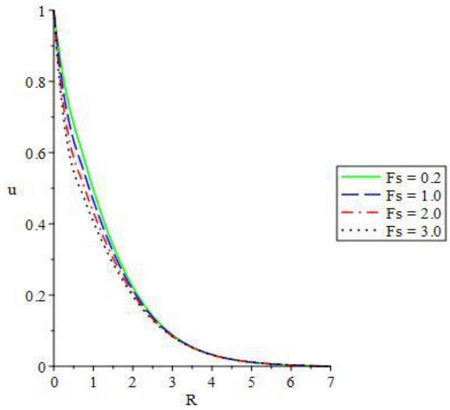

Fig. 9: Transient Velocity forvalues of Fs

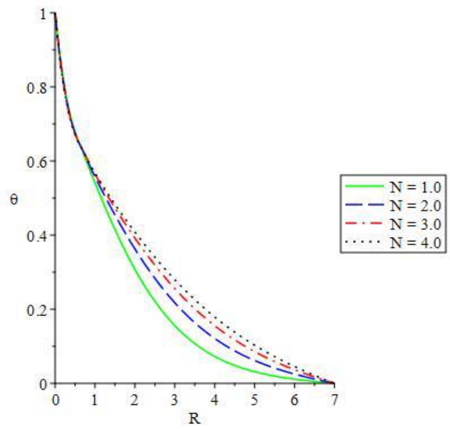

Fig. 10: Transient Temp. for values of N

Figure 9 depicts the reaction of Forchheimer parameter Fs on the velocity profiles. It is seen from the figure that the velocity profiles decrease with an increase in the values of Fs. This is due to the fact Forchheimer parameter Fs introduces a second order quadratic drag into the fluid flow in the cylinder which then causes a reduction in the flow velocity in the boundary layer. Fig. 10 represent the effect of an increase in the radiation parameter N on the heat energy transfer which leads to a rise in heat distribution within the boundary layer of the cylinder. Physically, a rise in N has a tendency to cause a rise in temperature at every point away from the surface and reduces the fluid bonding force strength, thus higher values of N implies higher surface heat flux.

The effect of the local skin friction at the wall of the cylinder with diverse values of M are shown in Figs. 11 and 12. From Fig. 13, a slight increase in the skin friction is observed close the surface but later decreases as it moves little distance from the cylinder surface between $0.5 \leq X \leq 2$ while it later rises as it keeps distance far away from the surface towards the free stream due looses in the fluid particles. Also, it is noticed in Fig. 12 that a rise in the values of M initially reduces the Nusselt effects quickly around the cylinder surface but it rises rapidly as it moves far from the surface towards the free stream in the boundary layer due to a sudden increase in the heat transfer within the system.

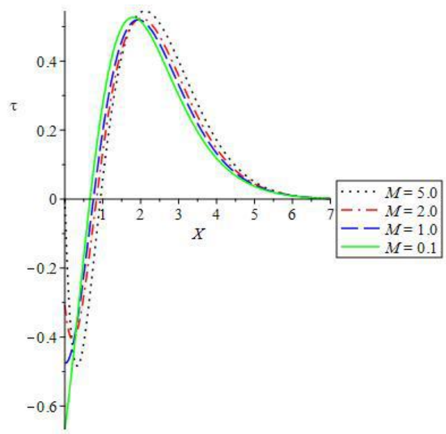

Fig. 11: Local Skin friction effects for values of M

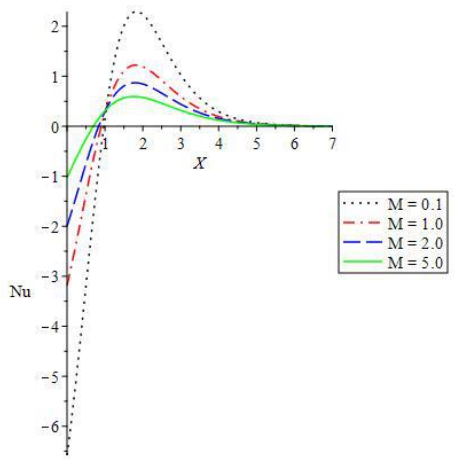

Fig. 12: Nusselt number effects for diverse values of M

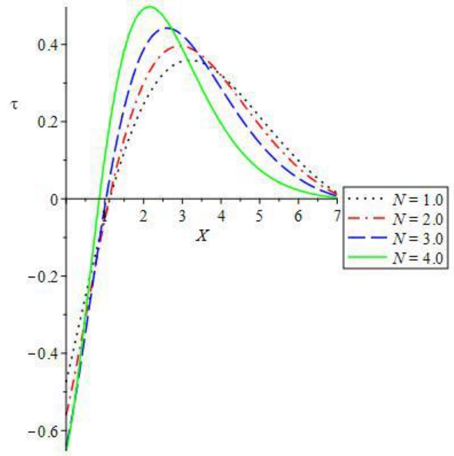

Fig. 13: Local Skin friction effects for values of N

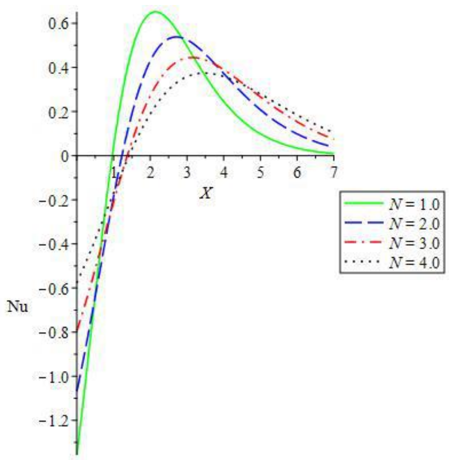

Fig. 14: Nusselt number effects for values of N

Figs. 13 and 14 show an initial increment from the negative state in the skin friction and Nusselt number due to early rises in the heat transfer in the cylinder but decreases gradually as it moves towards positive state around the plate surface as a result of a deceleration in the heat transfers rate in the system. But far away from the surface towards the free stream flow, the fluid temperature increases because the momentum and thermal boundary layer gets thicker as the radiation parameter values N rises and thereby causes increase in the effect of the skin friction and Nusselt number on the fluid flow in a cylinder.

Conclusion

In this research, a comprehensive computational analysis for unsteady free flow convective hydromagnetic ohmic heating in an inclined cylinder with heat under the effect of radiation, dissipation and Darcy-forchemier porous medium is considered by applying finite difference method of Crack-Nicolson type to solve the dimensionless boundary layer momentum and energy equations. The following conclusions are drawn from the study:

1. The fluid momentum fields decrease with an increase in the parameters values M, Da and Fs with the system.
2. Velocity profiles increase as the thermal Grashof number Gr and angle of inclination α of the cylinder increases.
3. The energy balance parameters λ and Ec enhances the energy distribution in the cylinder.
4. Prandtl number Pr retarded the transient temperature field in the cylinder.

Results obtained from this study will be helpful in the prediction of flow, heat transfer and solute or contaminant dispersion about intrusive bodies such as salt domes, magnetic intrusions, piping and casting systems.

Reference

Arora KL & Gupta PR 1972. Magnetohydrodynamic flows between two rotating coaxial cylinders under the radial magnetic field. *Physics of Fluids,* 15(6): 1146-1147.

Carnahan B, Luther HA & Wilkes JO 1969. Applied numerical methods, John Wiley Sons, New York.

Dulal P & Hiranmoy M 2012. Non-Darcian buoyancy driven heat and mass transfer over a stretching sheet in a porous medium with radiation and Ohmic heating. *Int. J. Nonlinear Sci*., 14: 115-123.

Emerly-Ashly F 1963. The effect of the magnetic field upon the free convection of a conducting fluid. *J. Heat Transfer,* 85(2): 119-124.

Evan LB, Reid RC & Drake EM 1968. Transient natural convection in a vertical cylinder. *A. I. Ch. E. J.,* 14: 251-261.

Gao Z, Fang P, Ding M & Jin N 2015. Multivariate weighted complex network analysis for characterizing nonlinear dynamic behavior in two-phase flow. *Exp. Therm. Fluid Sci.,* 60: 157-164.

Gao Z, Yang Y, Fang P, Jin N, Xia C & Hu L 2015. Multi-frequency complex network from time series for uncovering oil-water flow structure. *Scientific Reports,* 5: 8222.

Gao Z, Cai Q, Yang Y, Dang W & Zhang S 2016. Multiscale limited penetrable horizontal visibility graph for analyzing nonlinear time series. *Scientific Reports* 6: 35622.

Gao Z, Yang Y, Zhai L, Ding M & Jin N 2016. Characterizing slug to churn flow transition by using multivariate pseudo-Wigner distribution and multivariate multiscale entropy. *Chem. Eng. J.*, 291: 74-81.

Gao Z, Yang Y, Zhai L, Jin N & Chen G 2016. A four-sector conductance method for measuring and characterizing low-velocity oil-water two-phase flows. *IEEE Transactions on Instrumentation and Measurement,* 65: 1690-1697.

Hayat T, Qayyum S, Alsaedi A & Asghar S 2017. Radiation effects on the mixed convection flow induced by an inclined stretching cylinder with non-uniform heat source/sink. *PLOS ONE,* 12(4): 1 – 23.

Hayat T, Qayyum S, Alsaedi A & Shafiq A 2016. Inclined magnetic field and heat source/sink aspects inflow of nanofluid with nonlinear thermal radiation. *Int. J. Heat Mass Transfer,* 103, 99–107.

Hayat T, Qayyum S, Alsaedi A & Waqas M 2016. The radiative flow of tangent hyperbolic fluid with convective conditions and chemical reaction. *Eur. Phys. J. Plus,* 131: 422.

Hossain MA 1988. Simultaneous heat and mass transfer on oscillatory free convection boundary layer flow. *Int. J. Energy Res.,* 12: 205-206.

Ismail MN, Mohamadien GF & Umit DG 2012. Finite difference solution of radiation on unsteady free convective magnetohydrodynamic flow past a vertical cylinder with heat and mass transfer. *Physics of Flu-dyn,* 14: 1-18.

Kumari M & Nath G 1999. Development of two-dimensional boundary layer with an applied magnetic field due to the impulsive motion. *Indian J. Pure and Appl. Math.,* 30(7): 695-708.

Manyonge WA, Kiema DW & Iyaya CC 2012. Steady MHD poiseuille flow between two infinite parallel porous plates in an inclined magnetic field. *Int. J. Pure & Appl. Math.,* 76(5): 661-668.

Periyana GG & Ponnamma HR 2000. Unsteady free convection MHD flow past a vertical cylinder with heat and mass transfer. *Int. J. Therm. Sci.,* 39: 265-272.

Rajesh VO, Anwar B & Sridevi CH 2016. Finite difference analysis of unsteady MHD free convective flow over moving semi-infinite vertical cylinder with chemical reaction and temperature oscillation effects. *J. Appl. Fluid Mechanics,* 9(1): 157-167.

Salawu SO & Amoo SA 2016. Magnetohydrodynamics effects on radiative and dissipative heat transfer near a stagnation point with variable viscosity and thermal conductivity, *Comp. Info. Systems*, 7(4): 51-62.

Salawu SO & Fatunmbi EO 2017. Dissipative heat transfer of micropolar hydromagnetic variable electric conductivity fluid past inclined plate with joule heating and non-uniform heat generation. *Asian J. Physical & Chem. Sci.*, 2(1): 1-10.

Sheikholeslami M, Ganji DD, Javed MY & Ellahi R 2015. Effect of thermal radiation on magnetohydrodynamics nanofluid flow and heat transfer by means of a two-phase model. *J Magn. Magn Mater*, 374: 36-43.

Soundalgekar VM, Lahurikar RM, Pohanerkar SG & Birajdar NS 1994. Effects of mass transfer on the flow past an oscillating infinite vertical plate with constant heat flux. *J. Thermophy. & Aeromech.*, 1: 119-124.

Sugunamma V, Sandeep N, Krishna PM & Ramana B 2013. Inclined magnetic field and chemical reaction effects on flow over a semi-infinite vertical porous plate through a porous medium. *Communications in Applied Sciences,* 1(1): 1-24.

Velusamy K & Garg VK 1992. Transient natural convection over a heat generating vertical cylinder. *Int. J. Heat Mass Tran.*, 35: 1293-1306.

Zheng L, Zhang C, Zhang X & Zhang J 2013. Flow and radiation heat transfer of a nanofluid over a stretching sheet with velocity slip and temperature jump in a porous medium. *J. Franklin Inst.*, 2: 990-1007.